biomedicines

MDPI

Article

SLC41A1-Mediated Magnesium Homeostasis Imbalance Promotes Osteoarthritis Progression by Inducing Abnormal Interaction Between Synovial Macrophages and Chondrocytes

Zhiyong Yu [1,†], Zongli Cao [2,†], Junsong Zhang [1], Wei Lei [1], Shigang Gong [1], Yechang Hu [1], Donglin Wu [1], Zhibo Sun [1], Xinghui Liu [3,*] and Rong Chen [1,*]

[1] Department of Traumatic Orthopedics, Xiangyang Hospital of Traditional Chinese Medicine, Xiangyang Hospital Affiliated to Hubei University of Chinese Medicine, Xiangyang 441000, China
[2] Department of Endocrinology, Xiangyang Hospital of Traditional Chinese Medicine, Xiangyang Hospital Affiliated to Hubei University of Chinese Medicine, Xiangyang 441000, China
[3] School of Basic Medical Sciences, Hubei University of Arts and Science, Xiangyang 441000, China
* Correspondence: liuxinghui555@163.com (X.L.); chenrong201@126.com (R.C.)
† These authors contributed equally to this work.

Abstract

Background: Osteoarthritis (OA) is a widespread degenerative joint disorder accompanied by marked M1/M2 macrophage imbalance in synovial tissue. The pathological interaction between synovial macrophages and impaired chondrocytes remains poorly defined. This study aims to determine whether SLC41A1-mediated magnesium homeostasis disturbance accelerates OA progression by triggering aberrant crosstalk between these two cell populations. **Methods:** A monoiodoacetate (MIA)-induced rat OA model was used to validate the in vivo cartilage-protective effect of intra-articular magnesium intervention, with cartilage integrity and synovial SLC41A1 expression, macrophage polarization evaluated by hematoxylin-eosin (HE), safranin O (S-O) staining and immunofluorescence. SLC41A1 expression in M1/M2 macrophages and magnesium's regulatory effect on M1 were analyzed. After SLC41A1 knockdown, M2 phenotypic retention, magnesium homeostasis, mitochondrial function and chondrocyte degeneration markers in co-culture were further detected. **Results:** In the MIA-induced rat OA model, intra-articular magnesium injection significantly attenuated cartilage degeneration, reduced OARSI scores, suppressed chondrocyte apoptosis, upregulated Col2a1 and downregulated MMP13. Magnesium intervention also attenuated synovial hyperplasia, markedly downregulated aberrantly elevated SLC41A1 expression in the synovial/infrapatellar fat pad compartment and inhibited M1 pro-inflammatory macrophage polarization. In vitro, M1 macrophages exhibited lower intracellular magnesium and higher SLC41A1 expression than M2 macrophages, and this alteration was reversed by magnesium supplementation. SLC41A1 knockdown in macrophages attenuated their pro-oxidative, pro-apoptotic injury to co-cultured chondrocytes, restored mitochondrial function, preserved M2 anti-inflammatory phenotype and intracellular magnesium homeostasis in the IL-1β-activated co-culture system. **Conclusions:** SLC41A1 modulates macrophage magnesium homeostasis in the synovial/infrapatellar fat pad compartment, promotes pathological macrophage–chondrocyte crosstalk and OA progression, and serves as a potential magnesium-targeted OA intervention target.

Keywords: osteoarthritis; mitochondrial dysfunction; macrophages; chondrocyte; SLC41A1

Check for updates

Academic Editor: Elisa Belluzzi

Received: 10 September 2026
Revised: 18 October 2026
Accepted: 19 October 2026
Published: 28 October 2026

Copyright: © 2026 by the authors. Licensee MDPI, Basel, Switzerland. This article is an open access article distributed under the terms and conditions of the Creative Commons Attribution (CC BY) license.

1. Introduction

Osteoarthritis (OA) is a common degenerative disease in the elderly, with clinical manifestations including recurrent joint pain and dysfunction. The current field consensus defines OA as a chronic whole-joint disorder initiated by early biochemical and cellular alterations in synovial tissues, which trigger progressive histological and structural modifications that ultimately lead to pan-articular multi-tissue dysfunction, with pathological involvement spanning all major intra-articular structures, including articular cartilage, synovium, infrapatellar fat pad, subchondral bone, meniscus and ligaments [1]. The progression of OA is driven by intricate, bidirectional pathological crosstalk between sustained synovial inflammation and gradual cartilage degeneration [2]. Therefore, no effective method is currently available in the clinic to delay disease progression. Based on this background, accumulating evidence indicates that mitochondrial dysfunction is a key pathological driver of osteoarthritis, and restoring mitochondrial function in chondrocytes holds considerable therapeutic potential for OA [3].

During the progression of OA, mitochondrial dysfunction in chondrocytes impairs energy production, elevates reactive oxygen species (ROS), and disrupts calcium ion homeostasis, ultimately exacerbating intra-articular inflammation and promoting cartilage matrix degradation [4]. Conversely, intra-articular inflammatory factors, such as interleukin-1β (IL-1β), can induce chondrocyte mitochondrial dysfunction [5] and promote the release of mitochondrial DNA (mtDNA) [6]. Then, the released mtDNA promotes M1 macrophage polarization via the cyclic GMP-AMP synthase-stimulator of interferon genes (cGAS-STING) pathway [7,8]. In chronic inflammatory OA joints, synovial macrophages exhibit a polarization imbalance predominantly skewed toward the M1 phenotype, resulting in an elevated M1-to-M2 ratio. The increased proportion of M1 macrophages promotes the expression of catabolic factors such as matrix metalloproteinases (MMPs) and thrombospondin motifs (ADAMTS) through the secretion of pro-inflammatory cytokines, including IL-1β, IL-6 and tumor necrosis factor-α (TNF-α), ultimately leading to degradation of the cartilage extracellular matrix (ECM) [9,10]. This reciprocal amplification cascade between mitochondrial dysfunction in chondrocytes and M1 polarization of synovial macrophages serves as a core pathological driver of OA, offering a potential therapeutic target for intervening in OA progression.

Magnesium is an essential micronutrient that plays a fundamental role in maintaining metabolic homeostasis and systemic energy balance. Existing studies have confirmed that magnesium supplementation not only reduces chondrocyte apoptosis but also promotes chondrocyte proliferation and differentiation during articular cartilage repair [11]. Notably, combination therapy with magnesium ion (Mg^{2+}) and vitamin C has been shown to promote M2 polarization of synovial macrophages, which in turn attenuates OA-induced joint structural damage and chronic pain [12]. Mechanistically, Mg^{2+} modulates the polarization balance of macrophages toward the pro-inflammatory M1 or anti-inflammatory M2 phenotype by inducing cytoprotective autophagy [13]. Consistent with these reports, our previous work demonstrated that intra-operative irrigation with magnesium sulfate suppresses local inflammatory response and delays articular cartilage degeneration [14]. In line with these findings, solute carrier family 41 member 1 (SLC41A1) dysregulation-mediated intracellular Mg^{2+} imbalance is reported to drive lipopolysaccharide (LPS)-induced mitochondrial damage; conversely, exogenous Mg^{2+} supplementation can restore intracellular Mg^{2+} homeostasis, inhibit the opening of mitochondrial permeability transition pore (mPTP), and reduce the leakage of mtDNA and ROS [15]. Although Mg^{2+} is known to promote synovial macrophage M2 polarization and attenuate OA injury, the role of SLC41A1 in this magnesium-dependent process remains undefined. It is therefore critical to clarify whether aberrant SLC41A1 upregulation in synovial M1 macrophages blunts magnesium's

anti-inflammatory action, disrupts macrophage–chondrocyte homeostasis, and drives OA progression via an unrecognized magnesium-centered pathological amplifier. BaTiO3 modulates mitochondrial function by promoting MRS2-mediated mitochondrial Mg^{2+} influx, thereby inducing macrophage M2 polarization while suppressing M1 differentiation and osteoclastogenesis [16]. Whether Mg^{2+} exerts direct chondroprotective effects beyond general anti-inflammation, particularly by regulating chondrocyte mitochondrial function during OA progression, also remains poorly elucidated.

Therefore, this study investigated whether SLC41A1-mediated magnesium homeostasis disturbance promotes M2-to-M1 macrophage polarization, thereby driving a self-reinforcing cycle of pathological macrophage–chondrocyte crosstalk, cartilage mitochondrial damage, and sustained M1 macrophage activation, ultimately accelerating OA progression. We further examined whether SLC41A1 serves as a central mediator in magnesium homeostasis-regulated macrophage polarization and chondrocyte dysfunction. These findings aim to provide new mechanistic insights into the chondroprotective effects of magnesium and point to potential therapeutic strategies for OA in clinical practice.

2. Materials and Methods

2.1. Reagents

Magnesium sulfate ($MgSO_4$, 99.99% purity) was purchased from Shanghai Macklin Biochemical Co., Ltd. (Shanghai, China). The BCA protein assay kit, DAPI-containing antifade mounting medium, IL-1β, IL-6, TNF-α, TGF-β, IL-10 ELISA kits, ROS detection kit, JC-1 mitochondrial membrane potential assay kit, and TUNEL apoptosis detection kit were all obtained from Beyotime Biotechnology (Shanghai, China). High-glucose Dulbecco's modified Eagle's medium (DMEM) and fetal bovine serum (FBS) were supplied by Hyclone (Logan, UT, USA). The primary antibodies used in this study included anti-SLC41A1 (Thermo Fisher Scientific, Waltham, MA, USA), anti-iNOS (Santa Cruz Biotechnology, Dallas, TX, USA), anti-MMP13 (Proteintech, Rosemont, IL, USA), anti-type II collagen (Col2a1, HuaAn Biotechnology, Hangzhou, China), anti-CD206 (HuaAn Biotechnology) and anti-GAPDH (Fude Biological Technology, Hangzhou, China). The corresponding secondary antibodies, including horseradish peroxidase-conjugated goat anti-rabbit IgG, Cy3-conjugated goat anti-mouse IgG, and FITC-conjugated secondary antibodies, were all purchased from Proteintech. TRIzol reagent was obtained from Invitrogen (Carlsbad, CA, USA). The Mag-Fluo-4 AM intracellular magnesium fluorescent probe was supplied by Qiyuan Biotechnology (Shanghai, China). SOD2 and MDA ELISA kits were purchased from Fantai Biological (Shanghai, China). PrimeScript RT reagent Kit and qPCR SYBR® Green Master Mix were products of TaKaRa (Kusatsu, Japan).

2.2. Establishment and Grouping of Rat Osteoarthritis Model

Eight-week-old male Sprague-Dawley rats (SD) were supplied by the Animal Experimental Center of Hubei University of Medicine. All animal experiments were approved by the Institutional Animal Care and Use Committee of Hubei University of Medicine (No. 2021-033) and performed following the ARRIVE guidelines. After 7 days of acclimation, 18 rats were randomized into 3 groups (n = 6 per group): sham, OA, and Mg^{2+} treatment cohorts. Under isoflurane anesthesia, the right knee was routinely disinfected, flexed to 90°, and punctured via the medial parapatellar tendon to place the needle accurately inside the articular cavity. OA was induced by intra-articular injection of 50 μL monosodium iodoacetate (MIA) (1 mg in sterile saline), while the sham group received an equal volume of vehicle. The needle was left in situ for 10 s to avoid leakage, followed by 1 min of local compression for hemostasis. Post-operatively, animals were housed in a thermoregulated environment with ad libitum food and water. OA modeling success was verified by his-

tological evaluation of cartilage degeneration 14–28 days post-MIA injection. Two weeks after modeling, Mg^{2+} groups received twice-weekly (Monday and Thursday) intra-articular $MgSO_4$ injections (4.8 mg/kg, 100 μL), while the OA group received equivalent saline. All animals were euthanized at 8 weeks post-MIA injection, and joint tissues were harvested for downstream analyses.

2.3. Histological and Immunofluorescence Analysis

Isolated knee joint tissues (including the intact synovial/infrapatellar fat pad compartment and the medial femoral condyle cartilage-bearing region) were immediately fixed in 4% paraformaldehyde at 4 °C for 24 h. After thorough rinsing with phosphate-buffered saline, the specimens were subjected to standardized decalcification in 10% EDTA decalcifying solution at 4 °C for 14 days, with the decalcification endpoint confirmed by a needle puncture test. Following gradient serial dehydration with ethanol, the medial femoral condyle regions were paraffin-embedded, and 5 μm sagittal-oriented sections were generated. Consecutive sections were processed for hematoxylin and eosin (HE) staining, safranin O (S-O) staining, and immunofluorescence labeling. The degree of articular cartilage degeneration and synovial inflammation was blindly scored by two independent investigators using the validated OARSI (Osteoarthritis Research Society International) scoring system, following the established protocol described in reference [17]. For immunofluorescence staining, cartilage sections were blocked and then incubated with primary antibodies against Col2a1, MMP13, iNOS and SLC41A1 (all diluted at 1:200) at 4 °C overnight. After rinsing, sections were incubated with fluorophore-conjugated secondary antibodies (1:200) for 1 h at room temperature (25 °C) in the dark. Cell nuclei were counterstained with DAPI for 5 min at 25 °C, and images were acquired using a Leica fluorescence microscope (Leica Microsystems, Wetzlar, Germany). Quantitative analysis of fluorescence intensity was performed using Image J v2.1 software (National Institutes of Health, Bethesda, MD, USA).

2.4. Bioinformatic Reanalysis of Public GEO Transcriptomic Datasets

Three public GEO transcriptomic datasets were reanalyzed. GSE271903 contains synovial profiles from C57BL/6J mice, comparing ACLR-induced post-traumatic OA and age-matched sham groups. GSE305061 includes LPS-induced M1 RAW264.7 macrophages and unstimulated M0 controls. GSE290919 covers RAW264.7 M1 subsets induced by LPS plus interferon-γ, M2 subsets polarized with IL-4, IL-10, IL-13 and TGF-β1, and parallel M0 controls. All raw data were downloaded from GEO, processed with RMA normalization and $\log_2$ transformation, and annotated against the corresponding mouse genome platform. Differential expression analysis was performed in limma, with adjusted $p < 0.05$ and $|\log_2 FC| > 1$ set as the significance threshold. SLC41A1 expression was extracted across sham/OA synovium and M0/M1/M2 macrophage groups to clarify its polarization-specific transcriptional pattern in OA synovial macrophages.

2.5. Quantification of Cytokines and Oxidative Stress Biomarkers

Synovial/infrapatellar fat pad compartment tissue, cell homogenate supernatant and cell supernatant were collected for detecting IL-1β, IL-6, TNF-α, IL-10, TGF-β, SOD2 and MDA via validated commercial ELISA kits, strictly following the manufacturer's protocols. All frozen samples were thawed slowly on ice, and kit components were pre-equilibrated to room temperature. A standard curve ($R^2 > 0.99$) was generated with gradient-diluted standards. After 1 h incubation at 37 °C, plates were washed 5 times to remove non-specific binding. The chromogenic reaction was performed in the dark for 15 min and terminated with stop solution, and OD values at 450 nm were immediately read on a microplate

spectrophotometer (Leica Microsystems, Germany). Final concentrations were normalized to corresponding sample total protein content to eliminate loading deviation.

2.6. Polarization of RAW264.7 Murine Macrophages

RAW264.7 cells were cultured in high-glucose DMEM supplemented with 10% fetal bovine serum and 1% penicillin-streptomycin at 37 °C in a 5% CO_2 atmosphere. To avoid spontaneous polarization, cells between passages 5 and 10 were used. For M1 polarization, cells were seeded at a density of 2×10^5 cells per well in 6-well plates and grown to 60–70% confluence before stimulation with 1 μg/mL LPS for 24 h. The Mg^{2+} treatment group was supplemented with 5 mM magnesium sulfate in the conventional M1 culture medium. For M2 polarization, cells were seeded under the same conditions and treated with 20 ng/mL IL-4 and 20 ng/mL IL-13 for 24 h.

2.7. Lentiviral Transduction and Knockdown Validation

M1 and M2 polarized macrophages were transduced with lentiviral vectors to establish SLC41A1 knockdown. The experimental group received lentiviral particles encoding short hairpin RNA targeting SLC41A1 (SLC41A1-RNAi), while the control group was transduced with lentiviral particles carrying non-targeting control sequences (CON-RNAi). Three independent SLC41A1-targeting shRNAs (Sequence #1: 5′-GTCTCGAAAGATTGGGATCAA-3′; Sequence #2: 5′-GTCTTCACACCTGTGATTAAT-3′; Sequence #3: 5′-GGATCCCTGATGGCCACTTTA-3′) and non-targeting control lentivirus were obtained from Shanghai Gene Chemical Co., Ltd. (Shanghai, China). Transduction was performed according to the manufacturer's instructions. Briefly, macrophages were seeded in appropriate culture plates. When cells reached approximately 50–60% confluence, the culture medium was replaced with fresh medium containing lentiviral particles at the pre-optimized multiplicity of infection (MOI = 20) and 8 μg/mL polybrene. After 24 h of incubation, the virus-containing medium was replaced with fresh complete medium. Cells were then cultured for an additional 48–72 h to allow transgene expression before being used in subsequent experiments. Knockdown efficiency was validated at both the mRNA and protein levels 72–96 h post-transduction. Only cell populations demonstrating significant knockdown were used for downstream co-culture experiments.

2.8. Co-Culture System Establishment

M1–ATDC5 co-culture: Seed ATDC5 cells at a density of 1×10^5 cells/cm^2 in the lower chamber of a 0.4 μm pore-size Transwell system. Place the insert above and seed transfected M1 macrophages (SLC41A1-RNAi or CON-RNAi) into the insert at an appropriate ratio (5:1 M1 to ATDC5). M2–ATDC5 co-culture: Seed transfected M2 macrophages (SLC41A1-RNAi or CON-RNAi) at 2×10^5 cells/cm^2 in the lower chamber. Seed IL-1β-prestimulated ATDC5 chondrocytes at 1×10^5 cells/cm^2 into the Transwell insert placed on top.

2.9. Quantitative Real-Time PCR

Total RNA was isolated from M1 and M2 macrophages using TRIzol reagent (Invitrogen, Carlsbad, CA, USA) following the manufacturer's protocol. First-strand cDNA was synthesized from 1 μg of total RNA using the HiScript® III-RT SuperMix (Vazyme, Nanjing, China). Quantitative real-time PCR (qRT-PCR) was performed using the SYBR Green/ROX qPCR Master Mix (TaKaRa, Kusatsu, Shiga, Japan) on a CFX96 Real-Time PCR Detection System (Bio-Rad, Hercules, CA, USA). Gene-specific primers for *TRPM7*, *MAGT1*, *SLC41A1*, *SLC41A2*, *CNNM2* and *CNNM3* (sequences listed in Table 1) were used. Glyceraldehyde-3-phosphate dehydrogenase (GAPDH) served as the endogenous control. Each reaction was run in triplicate. The thermal cycling conditions were as follows: initial denaturation at 95 °C for 30 s, followed by 40 cycles of 95 °C for 5 s and 60 °C for 30 s. A

melt curve analysis was performed to confirm amplification specificity. The relative mRNA expression levels were calculated using the $2^{-\Delta\Delta C_T}$ method.

Table 1. Primers used for assessing the gene expressions using the qRT-PCR.

Gene	Forward (Sequence 5′-3′)	Reverse (Sequence 5′-3′)
Mouse TRPM7	TGACTCCACTCTCCCGACAATCTG	ATGATAAGAGGAGGAGGCAGGACTG
Mouse MAGT1	GATGGGCTTTTGCAGCTTTGT	GCAATACACATCATCCTTCGCT
Mouse SLC41A1	TACTGGCCCTACTCCTTCTCC	GGGACTCAATCACTACCACCTC
Mouse SLC41A2	CTTCAGCAAGAGATCAGAGCC	CCAGCATAGTCATCGTACTTGG
Mouse CNNM2	AAGTGGCCCACCGTGAAAG	CGCTTCTACTTCTGTTGCTAGG
Mouse CNNM3	GACTCCGGCACTGTCCTAGA	AGTGGATGGTTGTAGAAGCGG
Mouse GAPDH	ATGGGACGATGCTGGTACTGA	TGCTGACAACCTTGAGTGAAAT

2.10. Western Blot Analysis

Proteins were extracted with RIPA buffer plus inhibitors. Concentration was measured by BCA kit (Beyotime, Shanghai, China). Equal protein (30 μg) was separated on 10% SDS-PAGE, transferred to PVDF membrane, blocked with 5% milk, and incubated with anti-SLC41A1 (1:500) and anti-GAPDH (1:10,000) antibodies overnight at 4 °C. After TBST washes, membranes were incubated with HRP-secondary antibody (1:10,000) for 1 h at RT. Bands were visualized using ECL (Beyotime, China) on a Bio-Rad imager.

2.11. Immunofluorescence

Sterilized glass coverslips were placed in 6-well plates, onto which macrophages or chondrocytes were seeded. Following designated treatments, cells were fixed with 4% paraformaldehyde at 37 °C for 30 min, washed three times with PBS, and permeabilized with 0.3% Triton X-100 for 5 min at room temperature. Subsequently, cells were blocked with 5% fetal bovine serum for 30 min at 25 °C and incubated overnight at 4 °C with primary antibodies against iNOS, CD206, Col2a1, and MMP13. The next day, coverslips were washed with PBS and incubated with fluorescein-conjugated secondary antibody (1:200 dilution) for 1 h in the dark at 25 °C. Finally, nuclei were counterstained with DAPI for 5 min. After mounting with an anti-fade mounting medium, images were captured using a fluorescence microscope (Leica Microsystems, Germany). Fluorescence intensity was quantified using ImageJ software (version 2.1, Bethesda, MD, USA).

2.12. Intracellular Magnesium Concentration Detection

Intracellular Mg^{2+} levels were assessed using the fluorescent indicator Mag-Fluo-4 AM. Following the specified treatments, cells were incubated with 5 μM Mag-Fluo-4 AM in HBSS supplemented with 0.02% Pluronic F-127 for 45 min at 37 °C in the dark, and then allowed to de-esterify for an additional 30 min. Fluorescence imaging was performed using a Leica fluorescence microscope (Leica Microsystems, Germany).

2.13. Detecting Mitochondrial Function in ATDC5 Cells

Intracellular ROS detection: ATDC5 cells were loaded with the DCFH-DA probe (10 μM) at 37 °C for 20 min, washed, and the fluorescence intensity was quantified by fluorescence microscopy to reflect ROS levels.

Mitochondrial membrane potential assessment: Treated cells were incubated with JC-1 working solution at 37 °C for 20 min, washed, and analyzed. The ratio of red (aggregates, high ΔΨm) to green (monomers, low ΔΨm) fluorescence, determined by fluorescence microscopy, served as an indicator of mitochondrial health.

Apoptosis analysis by TUNEL staining: Cells were fixed with 4% paraformaldehyde, permeabilized with 0.1% Triton X-100, and incubated with TUNEL reaction mixture for

1 h at 37 °C in the dark. After DAPI counterstaining, TUNEL-positive cells were counted under a fluorescence microscope to calculate the apoptosis rate.

2.14. Statistical Analysis

All cellular assays were repeated ≥ 3 independent times. Data were analyzed in SPSS 25.0 (IBM, Armonk, NY, USA), presented as mean ± SD. The unpaired two-tailed Student's *t*-test was used for two-group comparisons and a one-way ANOVA with an LSD post hoc test for multiple groups. Statistical significance was defined as $p < 0.05$.

3. Results

3.1. Intraarticular Injection of Magnesium Exerts a Protective Effect on Cartilage and Slows the Progression of Osteoarthritis

Figure 1A provides a schematic overview of the stepwise experimental timeline. In the HE-stained sections shown in Figure 1B, the cartilage surface in the OA group appeared uneven, accompanied by chondrocyte loss and disorganized cellular arrangement. Notably, magnesium treatment partially attenuated these pathological changes. Consistently, the OARSI score was significantly elevated in the OA group, whereas it was reduced in the Mg^{2+}-treated group (Figure 1E). S-O staining revealed a similar pattern, revealing a pronounced loss of cartilage extracellular matrix glycosaminoglycans (GAGs) and proteoglycans in the OA group, whereas the Mg^{2+} group effectively suppressed this depletion (Figure 1B,E). As shown in Figure 1C,F, TUNEL staining revealed increased chondrocyte apoptosis in the OA group, whereas apoptosis was reduced in the Mg^{2+} group. Furthermore, double immunofluorescence staining for Col2a1 (green) and MMP13 (red) demonstrated opposing trends in signal intensity among all experimental groups (Figure 1D,G). Mg^{2+} treatment conferred significant cartilage-protective effects, as evidenced by markedly elevated Col2a1 fluorescence and a concurrent reduction in MMP13 signal.

3.2. Magnesium Ion Intervention Significantly Downregulates the Aberrant Expression of SLC41A1 in Synovial/Infrapatellar Fat Pad Compartment and Suppresses M1 Pro-Inflammatory Polarization of Macrophages

Representative HE images in Figure 2A show that the OA group presented with pronounced synovial/infrapatellar fat pad compartment thickening, accompanied by excessive fibroblast proliferation and massive inflammatory cell infiltration. Mg^{2+} intervention partially attenuated these changes, resulting in a lower synovial score compared to that of the OA group (Figure 2B). Double-label immunofluorescence staining was performed to detect the expression of SLC41A1 and the M1 macrophage marker iNOS in the synovial/infrapatellar fat pad compartment. The results revealed a concurrent increase in the fluorescence intensities of SLC41A1 and iNOS in the OA group, whereas Mg^{2+} treatment exerted a suppressive effect on both signals (Figure 2C,D). As illustrated in Figure 2E, the Mg^{2+} intervention group presented significantly downregulated expression of the pro-inflammatory mediators IL-1β, IL-6 and TNF-α, alongside markedly elevated expression of the anti-inflammatory cytokine IL-10, when compared with the untreated OA model group. Reanalysis of GSE271903 shows that SLC41A1 mRNA expression is significantly elevated in the ACLR-induced OA group compared with the sham group (Figure 2F). Consistently, independent reanalysis of GSE305061 and GSE290919 further demonstrates that SLC41A1 expression is markedly upregulated in M1-polarized RAW264.7 macrophages relative to M0, and in GSE290919, SLC41A1 expression is significantly higher in M1 than in M2 subsets (Figure 2G).

3.3. M1 Macrophage Polarization Links SLC41A1 Upregulation to Reduced Intracellular Magnesium, Partially Attenuated by Magnesium Supplementation

Mg^{2+} treatment not only increased the CD206 fluorescence intensity in M1 macrophages but also reduced their iNOS fluorescence intensity (Figure 3A–D). Compared with M2 macrophages, M1 macrophages exhibit reduced intracellular magnesium levels alongside increased protein expression of SLC41A1 (Figure 3E,F,H). Additionally, the levels of IL-10 and TGF-β in the cell supernatant are decreased, whereas IL-1β expression is elevated (Figure 3G). Notably, Mg^{2+} treatment in M1 macrophages can reverse this trend (Figure 3E–H). The heatmap of qRT-PCR results revealed that, among the magnesium ion-related pathway factors examined (*TRPM7*, *MAGT1*, *SLC41A1*, *SLC41A2*, *CNNM2*, and *CNNM3*), *SLC41A1* exhibited a marked increase in relative mRNA expression (Figure 3I).

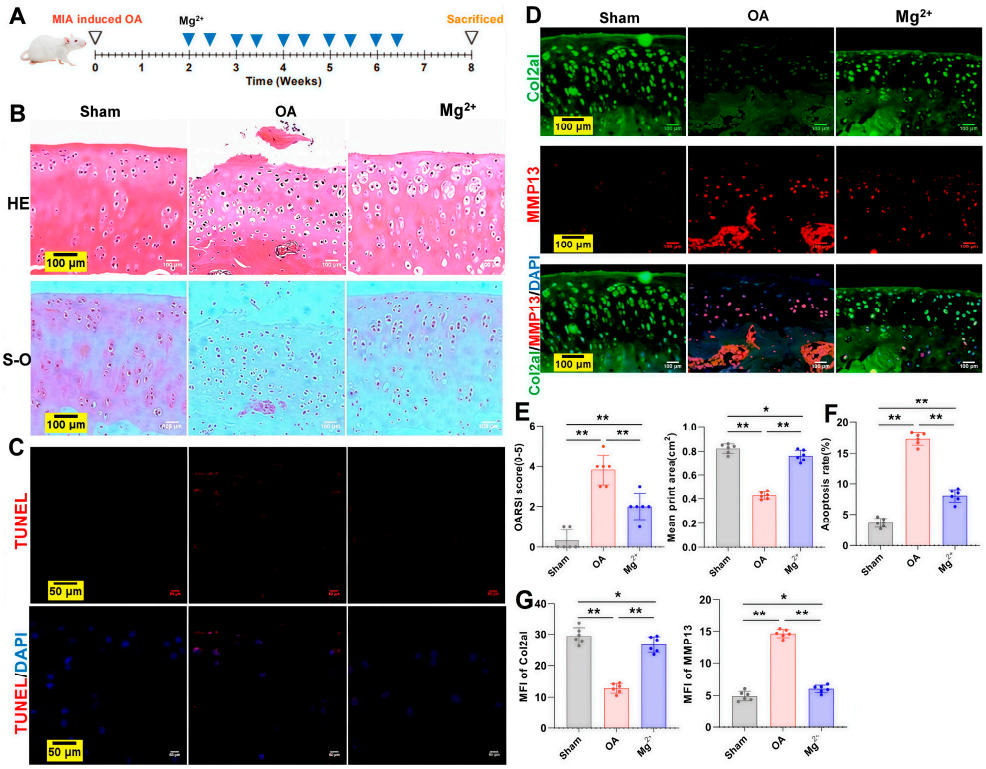


Figure 1. Intraarticular injection of magnesium exerts a protective effect on cartilage and slows the progression of osteoarthritis. (**A**) The stepwise experimental timeline. (**B**) Cartilage structural degradation was evaluated using hematoxylin-eosin (HE) and safranin O (S-O) staining. Scale bar: 100 μm. (**C**) TUNEL staining was performed to assess chondrocyte apoptosis. Scale bar: 100 μm. (**D**) The expression profiles of Col2a1 (green) and MMP13 (red) were characterized using an immunofluorescence staining protocol. Scale bar: 100 μm. (**E**) OA-associated histopathological alterations were assessed via the OARSI scoring system derived from HE staining and quantitative analysis of the mean print area (cm^2) of safranin O-positive glycosaminoglycan (GAG) regions in articular cartilage. (**F**) Quantitative analysis of the apoptosis rate, calculated as the percentage of TUNEL-positive chondrocyte area relative to the total DAPI-stained nuclear area across the full cartilage field of view. (**G**) The mean fluorescence intensity (MFI) of Col2a1 and MMP13 was determined from immunofluorescence staining. * $p < 0.05$, ** $p < 0.01$, $n = 6$ per group, one-way ANOVA with an LSD post hoc test.

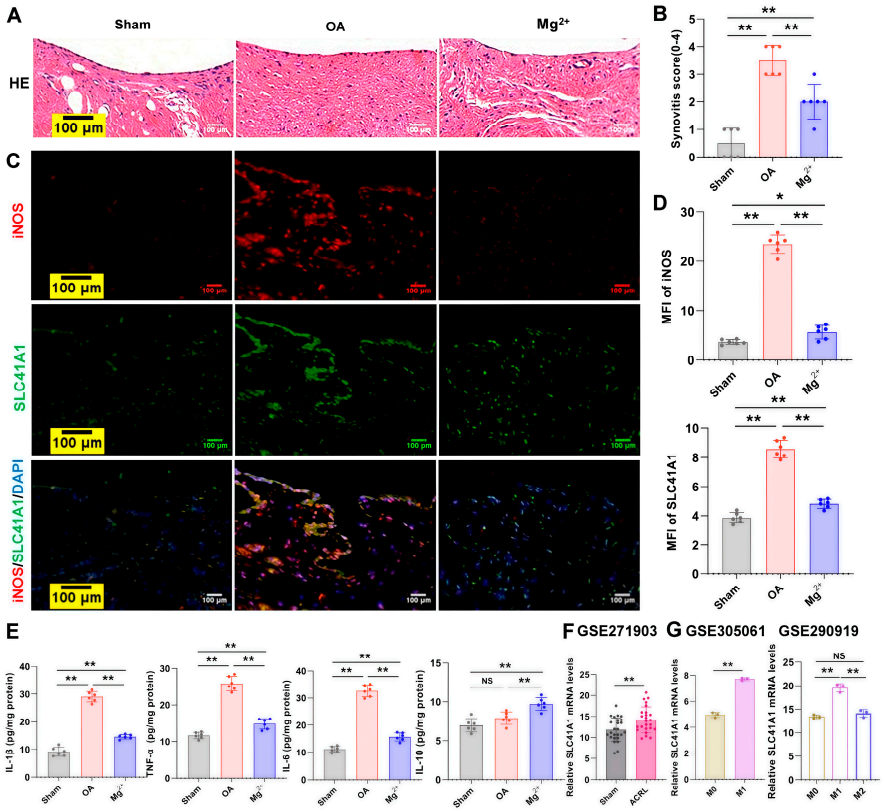


Figure 2. Magnesium ion intervention significantly downregulates the aberrant expression of SLC41A1 in the synovial/infrapatellar fat pad compartment and suppresses M1 pro-inflammatory polarization of macrophages. (**A**) Synovial/infrapatellar fat pad compartment inflammation was assessed using routine HE staining. Scale bar: 100 μm. (**B**) Synovitis histological scoring was completed based on HE-stained sections, $n = 6$ per group, one-way ANOVA with an LSD post hoc test. (**C**) Immunofluorescence labeling was performed to visualize the distribution of the pro-inflammatory M1 macrophage marker iNOS (red) and the magnesium efflux transporter SLC41A1 (green). Scale bar: 100 μm. (**D**) The mean fluorescence intensity (MFI) of target signals was quantitatively calculated from immunofluorescence images, $n = 6$ per group, one-way ANOVA with an LSD post hoc test. (**E**) The expression profiles of pro-inflammatory factors IL-1β, IL-6, TNF-α and anti-inflammatory cytokine IL-10 were determined via ELISA, $n = 6$ per group, one-way ANOVA with an LSD post hoc test. (**F**) *SLC41A1* mRNA expression in ACRL-induced OA and sham groups, reanalyzed from GSE271903. $n = 25$ per group, unpaired *t*-test. (**G**) *SLC41A1* mRNA expression in M1 versus M0 macrophages, reanalyzed from GSE305061 ($n = 3$ per group, unpaired *t*-test), and in M1, M2 and M0 macrophages, reanalyzed from GSE290919 ($n = 3$ per group, one-way ANOVA with an LSD post hoc test). * $p < 0.05$, NS $p > 0.05$, ** $p < 0.01$.

3.4. Knockdown of SLC41A1 Attenuates the Pro-Oxidative and Pro-Apoptotic Effects of M1 Macrophages on Co-Cultured Chondrocytes

Figure 4A outlines the experimental setup for co-culturing SLC41A1-RNAi-transfected M1 macrophages with ATDC5 chondrocytes. The knockdown efficiency of SLC41A1 RNAi in M1 macrophages was confirmed at the protein level. Both the second and third transfection systems produced significant silencing effects (Figure 4B,C), and the qRT-PCR results were consistent with the protein data (Figure 4D). The second and third transfection systems produced comparable significant SLC41A1 silencing, with no statistical difference. The third system was selected for subsequent experiments, as it showed a trend toward slightly lower residual SLC41A1 expression across all preliminary validation tests. Compared to the control group, co-culture with SLC41A1-knockdown M1 macrophages resulted in significantly reduced ROS production (Figure 4E,F), a decrease in TUNEL-positive apoptotic cells (Figure 4G,H), elevated mitochondrial membrane potential as

indicated by JC-1 staining (Figure 4I,J), downregulated MMP13 expression and upregulated Col2a1 expression in ATDC5 chondrocytes (Figure 4K,L). Additionally, the expression of the antioxidant enzyme SOD2 was increased, while the lipid peroxidation marker MDA was decreased (Figure 4M).

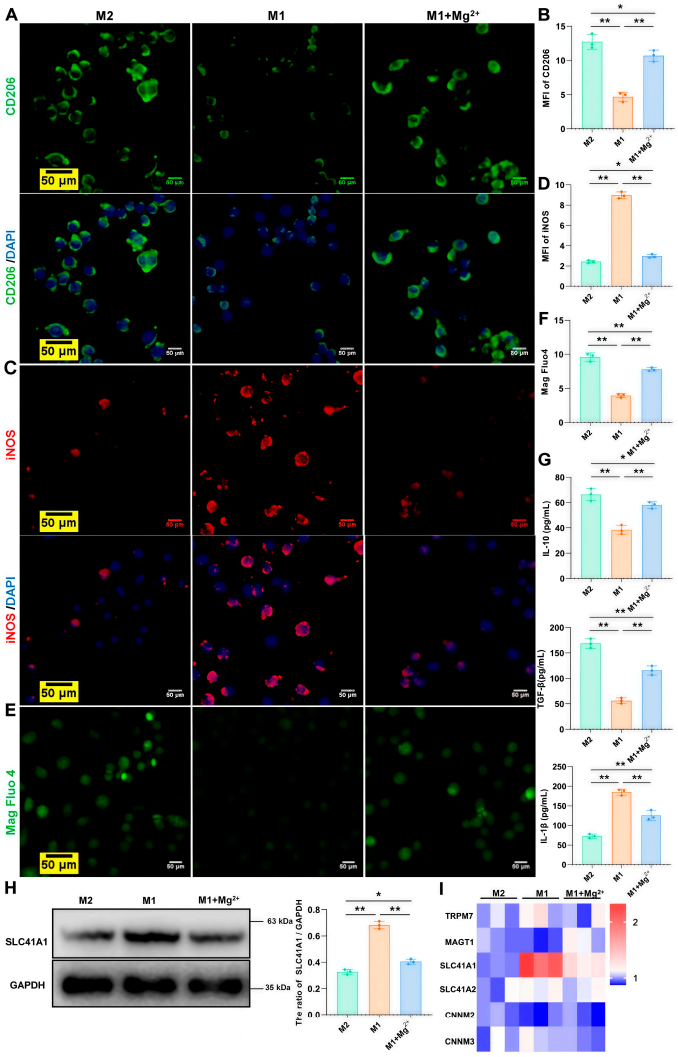


Figure 3. M1 macrophage polarization links SLC41A1 upregulation to reduced intracellular magnesium, partially attenuated by magnesium supplementation. (**A**) Immunofluorescence staining for the M2 macrophage surface marker CD206 (green). Scale bar: 50 μm. (**B**) Mean fluorescence intensity quantification of the M2 marker CD206. (**C**) Immunofluorescence detection of the M1 macrophage marker iNOS (red). Scale bar: 50 μm. (**D**) Mean fluorescence intensity analysis of the iNOS signal. (**E**) Intracellular magnesium flux was visualized using Mag Fluo4. Scale bar: 50 μm. (**F**) Quantitative evaluation of intracellular magnesium. (**G**) Cytokine profiles, including IL-10, TGF-β and IL-1β, were measured by ELISA. (**H**) The protein expression level of SLC41A1 was assessed via Western blot. (**I**) Hierarchical clustering heatmap illustrating mRNA expression patterns of magnesium transport-related genes (*TRPM7*, *MAGT1*, *SLC41A1*, *SLC41A2*, *CNNM2* and *CNNM3*) from qRT-PCR analysis. * $p < 0.05$, ** $p < 0.01$; $n = 3$ per group; one-way ANOVA with an LSD post hoc test.

3.5. SLC41A1 Knockdown Preserves M2 Macrophage Phenotype and Magnesium Homeostasis in IL-1β-Activated Chondrocyte Co-Culture

As illustrated in Figure 5A, the experimental setup involved co-culturing IL-1β-induced ATDC5 chondrocytes with M2 macrophages in which SLC41A1 expression was knocked down via RNA interference. Compared to the control, silencing SLC41A1 in M2 macrophages within the IL-1β-induced chondrocyte co-culture environment led to a series

of beneficial changes: restoration of intracellular magnesium homeostasis (Figure 5B,C), enhanced expression of the M2 polarization marker CD206 and suppression of the M1 marker iNOS (Figure 5D,E). This phenotypic shift was accompanied by a favorable alteration in the cytokine profile, characterized by increased secretion of IL-10 and TGF-β and decreased release of IL-1β and TNF-α (Figure 5F).

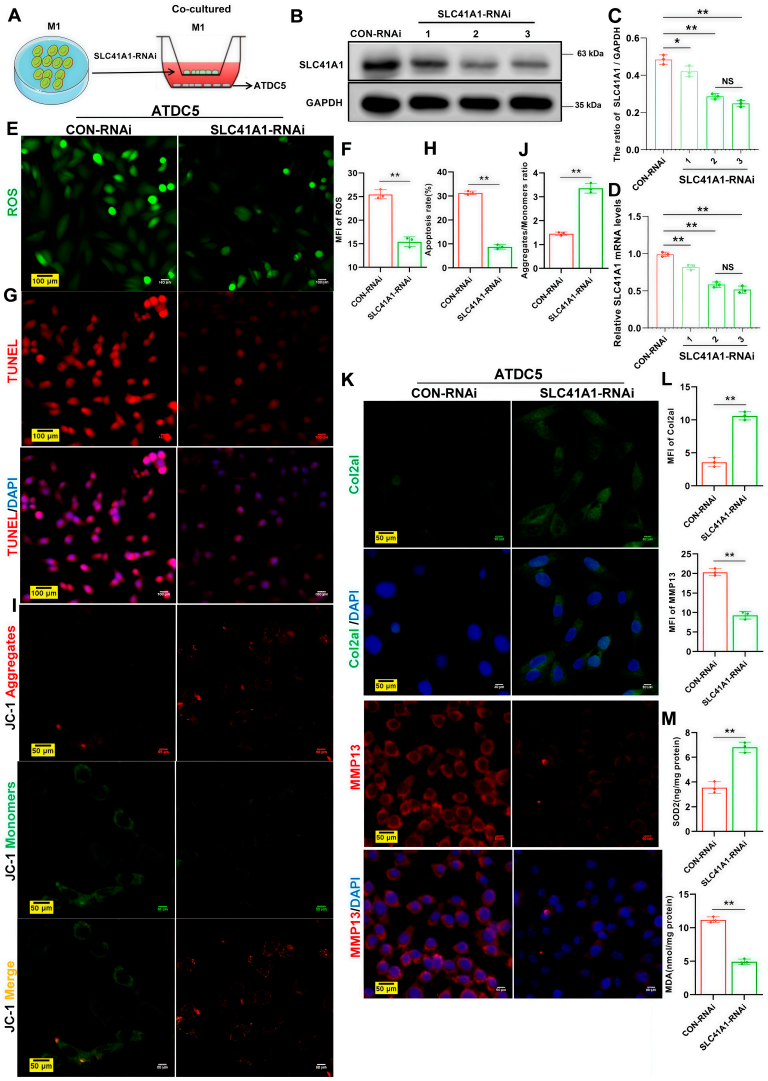


Figure 4. Knockdown of SLC41A1 attenuates the pro-oxidative and pro-apoptotic effects of M1 macrophages on co-cultured chondrocytes. (**A**) Schematic illustration of the experimental setup for co-culturing ATDC5 chondrocytes with SLC41A1-knockdown M1 macrophages. (**B**,**C**) The relative protein expression level of SLC41A1 in different experimental groups was quantified via Western blot analysis. (**D**) The relative mRNA levels of SLC41A1 were quantitated by qRT-PCR. (**E**) Intracellular reactive oxygen species (ROS) levels in chondrocytes were visualized using the DCFH-DA fluorescent probe. Scale bar: 100 μm. (**F**) Quantitative analysis of the relative fluorescence intensity for intracellular ROS. (**G**) Apoptotic chondrocytes were detected by TUNEL staining. Scale bar: 100 μm. (**H**) The apoptosis rate was calculated based on the percentage of TUNEL-positive cells. (**I**) Mitochondrial membrane potential in chondrocytes was assessed using the JC-1 fluorescent probe. Scale bar: 50 μm. (**J**) The ratio of JC-1 aggregates (red) to monomers (green) was calculated to represent mitochondrial membrane potential integrity. (**K**) Immunofluorescence staining was performed to localize the anabolic marker Col2a1 (green) and the catabolic enzyme MMP13 (red) in chondrocytes. Scale bar: 50 μm. (**L**) The mean fluorescence intensity of Col2a1 and MMP13 was quantitatively evaluated. (**M**) The activity of the antioxidant enzyme superoxide dismutase 2 (SOD2) and the content of the lipid peroxidation marker malondialdehyde (MDA) were measured using commercial assay kits. * $p < 0.05$, NS $p > 0.05$, ** $p < 0.01$; $n = 3$ per group; unpaired *t*-test.

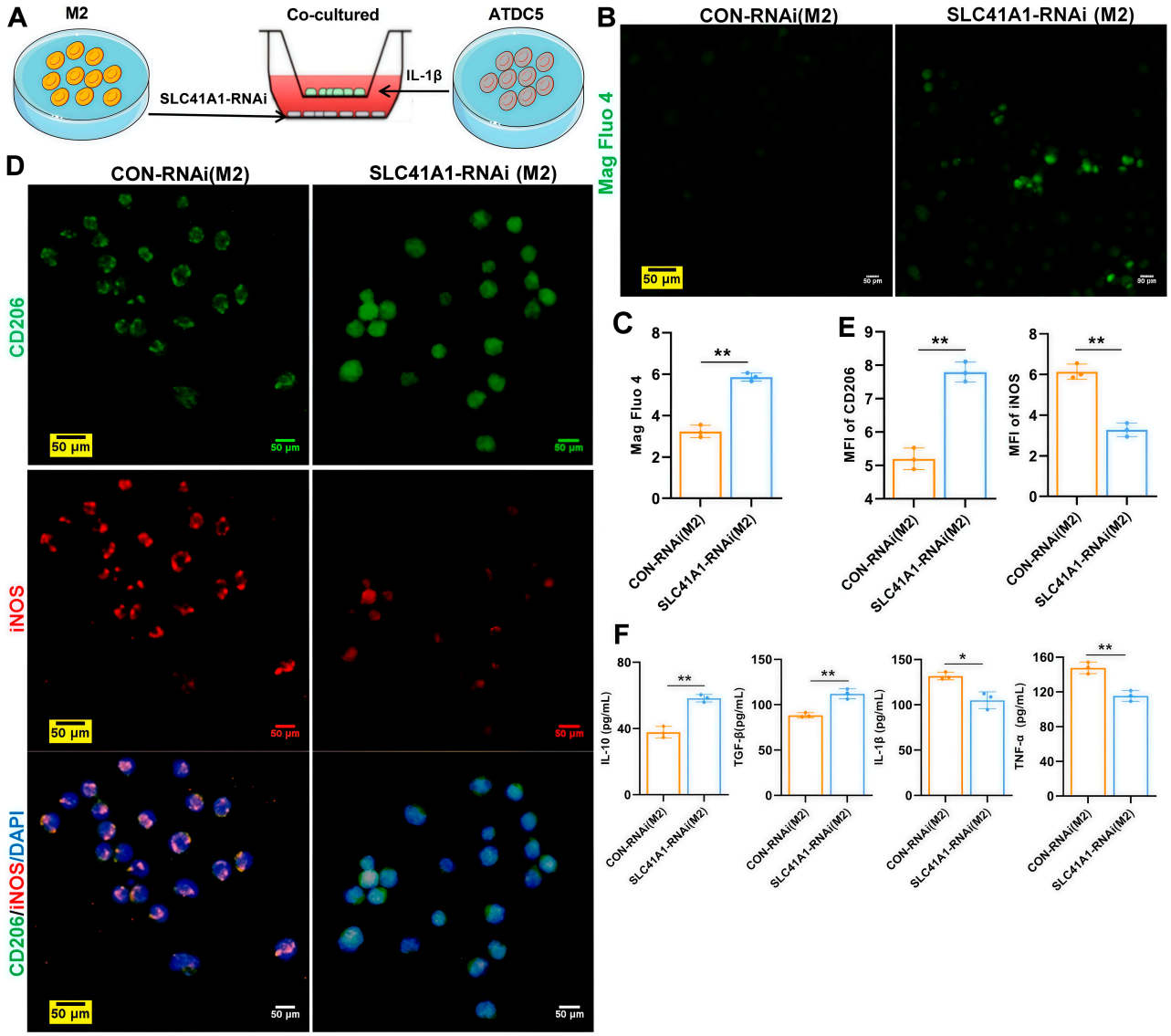


Figure 5. SLC41A1 knockdown preserves the M2 macrophage phenotype and magnesium homeostasis in IL-1β-activated chondrocyte co-culture. (**A**) Schematic representation of the experimental setup for co-culturing IL-1β-induced ATDC5 chondrocytes with SLC41A1-knockdown M2 macrophages. (**B**) Intracellular magnesium flux was visualized using Mag Fluo4. Scale bar: 50 μm. (**C**) Quantitative evaluation of intracellular magnesium. (**D**) Immunofluorescence staining was performed to co-localize CD206 (green) and iNOS (red). Scale bar: 50 μm. (**E**) The mean fluorescence intensity of CD206 and iNOS was quantitatively evaluated. (**F**) Cytokine profiles, including IL-10, TGF-β, IL-1β, and TNF-α, were measured by ELISA. * $p < 0.05$, ** $p < 0.01$; $n = 3$ per group; unpaired *t*-test.

4. Discussion

During the pathological progression of OA, articular chondrocytes consistently manifest progressive mitochondrial dysfunction, characterized by reduced mitochondrial membrane potential, excessive accumulation of mitochondria-derived ROS and impaired oxidative phosphorylation [18]. Although articular chondrocytes predominantly rely on glycolysis as their core energy supply pathway under physiological conditions, intact mitochondria remain indispensable for multiple critical cellular processes, including intracellular redox homeostasis maintenance, apoptotic cascade regulation, calcium signal transduction and cellular stress response [3]. Accumulating evidence has further confirmed that dysregulated mitochondrial function is causally and tightly linked to the core pathological phenotypes of OA chondrocytes, including aberrant apoptosis, cellular senescence, and

accelerated extracellular matrix catabolism [3,4,19]. As a low-grade chronic inflammatory joint disease, OA is pathologically driven by a self-perpetuating loop centered on aberrant synovium–cartilage crosstalk: pro-inflammatory cytokines and extracellular vesicles from synovial resident cells and infiltrating M1 macrophages initiate progressive cartilage ECM degradation, while accumulated cartilage breakdown fragments in turn trigger synovial hyperplasia and reinforce persistent M1 polarization [20]. At a subcellular level, excessive ROS and nitric oxide generated by overactivated M1 macrophages can directly target chondrocyte mitochondria, inducing mitochondrial DNA damage, respiratory chain dysfunction and impaired mitochondrial dynamics, which together exacerbate chondrocyte metabolic imbalance and cartilage degenerative phenotypes [19]. Therefore, effective OA prevention and treatment should not only focus on restoring chondrocyte mitochondrial function but also target persistently overactivated synovial M1 macrophages, whose sustained release of pro-inflammatory and oxidative mediators acts as a persistent extrinsic source of mitochondrial damage that cannot be eliminated by a single mitochondrial-targeted intervention alone.

Calcium influx serves as a critical upstream trigger for synovial M1 macrophage overactivation, which subsequently promotes chondrocyte apoptotic signaling transduction and ultimately accelerates the pathological progression of OA [21]. As a natural physiological calcium antagonist, magnesium ions (Mg^{2+}) have been verified to exert anti-inflammatory effects and yield significant cartilage-protective outcomes through intra-articular administration [14,22]; however, the precise cellular targets of action and the full downstream molecular regulatory networks underlying these therapeutic benefits remain to be systematically clarified. Accumulating anatomical and biochemical evidence confirms that the synovium and infrapatellar fat pad, connected by direct anatomical insertion sites and undergoing coordinated inflammatory remodeling, act as one integrated anatomofunctional unit—a feature that makes clean macro-dissection of the two separate tissues technically unfeasible during routine sampling [23]. Our experimental findings demonstrate that SLC41A1 and the M1 macrophage marker iNOS are significantly upregulated in the synovial/infrapatellar fat pad compartment in the OA group, and that this upregulation can be effectively attenuated by intra-articular administration of Mg^{2+}. SLC41A1 is a major Mg^{2+} efflux system that functions as a Na^{+}/Mg^{2+} exchanger, and its dysregulation is associated with diseases such as Parkinson's disease, pulmonary arterial hypertension and various cancers [24]. Following the intracellular entry of Mg^{2+} into macrophages, the excessively hyperactive inflammatory response can be significantly mitigated [25]. Our experimental data further confirm that M1 macrophages exhibit reduced intracellular Mg^{2+} content alongside marked upregulation of SLC41A1 expression, and exogenous magnesium supplementation partially attenuates these pathological alterations. In mice, exercise downregulates SLC41A1, and this effect is further amplified by magnesium supplementation [26]. Therefore, SLC41A1 may represent a previously unrecognized pathological amplifier in synovial M1 macrophages during OA progression: its aberrant upregulation drives sustained intracellular Mg^{2+} efflux, which in turn removes the physiological braking effect of magnesium on pro-inflammatory signaling cascades. The available literature further confirms the plausibility of this mechanism: SLC41A1 knockdown restricts excessive Mg^{2+} efflux, which not only alleviates pathological cardiac fibrosis [27] but also promotes matrix mineralization during the osteogenic differentiation of mesenchymal stromal cells [28].

In osteoarthritis, synovial M1 macrophage enrichment and concurrent M2 macrophage depletion jointly elevate local pro-inflammatory mediator release [29]. This established M1/M2 polarization imbalance acts not in isolation but as a core upstream signal propagating pathological changes across the multifactorial OA microenvironment to promote progressive synovial fibrosis [30]. Prior hepatocellular carcinoma studies have linked SLC41A1

upregulation to increased macrophage infiltration in the tumor immune niche [31]. Our independent analysis of two public macrophage transcriptome datasets, GSE305061 and GSE290919, further confirms that SLC41A1 is specifically upregulated in M1 versus M0 macrophages, supporting the functional role of this magnesium transporter in inflammatory macrophage activation. Co-culture of M1 macrophages with chondrocytes potently suppresses core chondrogenic gene expression (Col2a1, ACAN, SOX9), while markedly upregulating catabolic proteases including MMP13 and ADAMTS5 [32]. Our experimental results demonstrate that co-culturing chondrocytes with SLC41A1-knockdown M1 macrophages significantly upregulates the chondrogenic marker Col2a1 while concurrently suppressing the expression of the cartilage catabolic protease MMP13. Further mechanistic validation reveals that SLC41A1 knockdown in M1 macrophages confers protective effects on co-cultured chondrocytes, including the suppression of apoptotic progression, reduction of the lipid peroxidation biomarker MDA, and elevation of the antioxidant enzyme SOD2. Consistent with previously published reports that chondrocytes exposed to M1 macrophage-derived conditioned medium exhibit BAX upregulation, BCL2 downregulation, and aggravated apoptotic injury [33], our additional data confirm that the SLC41A1-knockdown M1 macrophage group in the co-culture system exhibits markedly lower intracellular ROS levels and a restored, higher mitochondrial membrane potential. LPS induces the upregulation of SLC41A1, which drives excessive Mg^{2+} efflux and subsequently triggers mitochondrial damage. Either SLC41A1 knockdown or exogenous Mg^{2+} supplementation can restore intracellular Mg^{2+} homeostasis, inhibit mPTP opening and restrict the leakage of mtDNA and ROS [14]. A growing body of preclinical evidence demonstrates that targeted ROS scavenging in chondrocytes preserves mitochondrial functional integrity and mitigates local inflammatory cascades, ultimately decelerating the pathological progression of OA [34–36]. IL-1β-driven mitochondrial injury in chondrocytes creates a pathological microenvironment that further promotes the pro-inflammatory M1 shift of M2 macrophages [4]. In our co-culture experimental system, SLC41A1-knockdown M2 macrophages display significantly elevated intracellular Mg^{2+} levels, and this sustained magnesium retention effectively protects the cells from undergoing the M2-to-M1 pro-inflammatory polarization transition. Magnesium-incorporated composite biomaterials exert dual protective effects: they not only clear excess intracellular ROS via sustained magnesium ion release but also trigger M2 phenotypic polarization in synovial macrophages [37,38].

Collectively, this study identifies SLC41A1 as a novel pathological mediator in the osteoarthritic synovial/infrapatellar fat pad compartment. SLC41A1 knockdown in M1 macrophages preserves chondrocyte mitochondrial function, while its inhibition in M2 macrophages sustains high intracellular Mg^{2+} levels and alleviates the M2-to-M1 pro-inflammatory shift. These findings reveal a new mechanistic basis for the chondroprotective effect of magnesium supplementation in OA. Nevertheless, several limitations should be noted. First, all functional results are derived from partial SLC41A1 knockdown without overexpression or rescue validation, which limits the causal interpretation of SLC41A1 as a core driver. Second, the exact downstream effectors of this SLC41A1-Mg^{2+} axis remain uncharacterized. Future work will validate these findings in cell-type-specific in vivo genetic models to support translational development of SLC41A1-targeted OA interventions.

5. Conclusions

This study identifies SLC41A1 in the synovial/infrapatellar fat pad compartment as a potential modulator linked to OA progression through altered macrophage–chondrocyte crosstalk. Elevated SLC41A1 expression in M1 macrophages leads to magnesium efflux,

which subsequently impairs chondrocyte mitochondrial function and contributes to cartilage degradation. Experimental evidence shows that magnesium supplementation in vivo attenuates OA damage and lowers SLC41A1, while SLC41A1 knockdown in vitro protects chondrocytes and sustains anti-inflammatory M2 macrophages. Targeting the SLC41A1–magnesium axis in this compartment may represent a plausible therapeutic strategy for OA by interrupting this pathogenic cell–cell communication.

Author Contributions: Conceptualization, Z.Y., Z.C., X.L. and R.C.; methodology, Z.Y., W.L. and Y.H.; software, Z.C., J.Z., S.G. and Y.H.; validation, Z.C. and X.L.; formal analysis, X.L. and R.C.; investigation, Z.C.; resources, J.Z., W.L. and D.W.; data curation, Z.Y. and Z.C.; writing—original draft, R.C.; writing—review and editing, X.L.; visualization, R.C.; supervision, Z.Y. and Z.S.; project administration, S.G., D.W., X.L. and R.C.; funding acquisition, Z.Y., Z.S., X.L. and R.C. All authors have read and agreed to the published version of the manuscript.

Funding: This work was supported by Hubei Provincial Natural Science Foundation (Grant Nos. 2025AFD051 and 2025AFD078), Hubei Provincial Natural Science Foundation Xiangyang Innovation and Development Joint Fund (Grant No. JCZRLH202601514), the Collaborative Clinical Project of Traditional Chinese Medicine and Western Medicine for Major Difficult and Critical Diseases in Hubei Province (Grant No. XYZY2024P01) and the Xiangyang Traditional Chinese Medicine Hospital Internal Fund (Grant No. XYZY2024G01).

Institutional Review Board Statement: All animal experiments in this study were reviewed and approved by the Institutional Animal Care and Use Committee (IACUC) of Hubei University of Medicine (Approval No. 2021-033, approved on 1 March 2021.) All procedures were strictly performed in full compliance with the ARRIVE (Animal Research: Reporting of In Vivo Experiments) guidelines, to ensure the welfare and ethical treatment of all experimental animals.

Informed Consent Statement: Not applicable.

Data Availability Statement: The data sets generated and analyzed during the current study are available from the corresponding authors on reasonable request.

Acknowledgments: This work was supported by the 2025 Demonstration Project for Reform and High-Quality Development of National Public Hospitals, which was initiated by the Department of Public Hospital Reform and Institutional Reform, National Health Commission of the People's Republic of China (Official Document No. 3, 2025) and undertaken by Xiangyang Hospital of Traditional Chinese Medicine. The authors extend sincere appreciation to all project participants for their on-site coordination and data support during the research process. During the preparation of this manuscript, the authors used Wenxin Yiyan (ERNIE Bot, version 4.0) for the purposes of polishing English expression, standardizing academic wording and checking reference format consistency. The authors have reviewed and edited the full AI-generated output, confirmed the accuracy of all factual statements, research conclusions and institutional information and take full responsibility for the final content of this publication.

Conflicts of Interest: The authors declare no conflicts of interest.

References

1. Yao, Q.; Wu, X.; Tao, C.; Gong, W.; Chen, M.; Qu, M.; Zhong, Y.; He, T.; Chen, S.; Xiao, G. Osteoarthritis: Pathogenic signaling pathways and therapeutic targets. *Signal Transduct. Target. Ther.* **2023**, *8*, 56. [CrossRef] [PubMed]
2. Sanchez-Lopez, E.; Coras, R.; Torres, A.; Lane, N.E.; Guma, M. Synovial inflammation in osteoarthritis progression. *Nat. Rev. Rheumatol.* **2022**, *18*, 258–275. [CrossRef] [PubMed]
3. Zhang, M.; Wu, J.; Cai, K.; Liu, Y.; Lu, B.; Zhang, J.; Xu, J.; Gu, C.; Chen, T. From dysfunction to healing: Advances in mitochondrial therapy for Osteoarthritis. *J. Transl. Med.* **2024**, *22*, 1013. [CrossRef] [PubMed]
4. Poznyak, A.V.; Orekhov, N.A.; Churov, A.V.; Starodubtseva, I.A.; Kovyanova, T.I.; Pecherina, T.B.; Sukhorukov, V.N.; Orekhov, A.N. Connection Between Mitochondria and Rheumatoid Arthritis and Osteoarthritis: Personalized Treatment Strategies. *Curr. Pharm. Des.* **2026**, *32*, 651–665. [CrossRef] [PubMed]

5. Eitner, A.; Müller, S.; König, C.; Wilharm, A.; Raab, R.; Hofmann, G.O.; Kamradt, T.; Schaible, H.G. Inhibition of Inducible Nitric Oxide Synthase Prevents IL-1β-Induced Mitochondrial Dysfunction in Human Chondrocytes. *Int. J. Mol. Sci.* **2021**, *22*, 2477. [CrossRef] [PubMed]
6. Seewald, L.A.; Sabino, I.G.; Montney, K.L.; Delco, M.L. Synovial fluid mitochondrial DNA concentration reflects the degree of cartilage damage after naturally occurring articular injury. *Osteoarthr. Cartil.* **2023**, *31*, 1056–1065. [CrossRef] [PubMed]
7. Guo, Y.; You, Y.; Shang, F.F.; Wang, X.; Huang, B.; Zhao, B.; Lv, D.; Yang, S.; Xie, M.; Kong, L.; et al. iNOS aggravates pressure overload-induced cardiac dysfunction via activation of the cytosolic-mtDNA-mediated cGAS-STING pathway. *Theranostics* **2023**, *13*, 4229–4246. [CrossRef] [PubMed]
8. Kim, D.; Jin, J.; Lee, Y.R.; Kim, D.H.; Park, S.Y.; Byun, J.K.; Choi, Y.K.; Park, K.G. SLC25A33-mediated mitochondrial DNA synthesis plays a critical role in the inflammatory response of M1 macrophages by contributing to mitochondrial ROS and VDAC oligomerization. *Int. J. Biol. Sci.* **2025**, *21*, 2935–2953. [CrossRef] [PubMed]
9. Zhao, K.; Ruan, J.; Nie, L.; Ye, X.; Li, J. Effects of synovial macrophages in osteoarthritis. *Front. Immunol.* **2023**, *14*, 1164137. [CrossRef] [PubMed]
10. Zhang, H.; Lin, C.; Zeng, C.; Wang, Z.; Wang, H.; Lu, J.; Liu, X.; Shao, Y.; Zhao, C.; Pan, J.; et al. Synovial macrophage M1 polarisation exacerbates experimental osteoarthritis partially through R-spondin-2. *Ann. Rheum. Dis.* **2018**, *77*, 1524–1534. [CrossRef] [PubMed]
11. Kuang, X.; Chiou, J.; Lo, K.; Wen, C. Magnesium in joint health and osteoarthritis. *Nutr. Res.* **2021**, *90*, 24–35. [CrossRef] [PubMed]
12. Yao, H.; Xu, J.; Wang, J.; Zhang, Y.; Zheng, N.; Yue, J.; Mi, J.; Zheng, L.; Dai, B.; Huang, W.; et al. Combination of magnesium ions and vitamin C alleviates synovitis and osteophyte formation in osteoarthritis of mice. *Bioact. Mater.* **2021**, *6*, 1341–1352. [CrossRef] [PubMed]
13. Zhu, Y.; Zhao, S.; Cheng, L.; Lin, Z.; Zeng, M.; Ruan, Z.; Sun, B.; Luo, Z.; Tang, Y.; Long, H. Mg(2+)-mediated autophagy-dependent polarization of macrophages mediates the osteogenesis of bone marrow stromal stem cells by interfering with macrophage-derived exosomes containing miR-381. *J. Orthop. Res.* **2022**, *40*, 1563–1576. [CrossRef] [PubMed]
14. Liu, X.; Chen, R.; Jiang, L.; Li, X.; Sun, Z. Effect of infusion irrigation with different irrigating solutions on transient receptor potential vanilloid 5 and intra-articular inflammation in a post-traumatic osteoarthritis rabbit model. *Eur. J. Med. Res.* **2021**, *26*, 24. [CrossRef] [PubMed]
15. Liu, Y.; Song, C.; Zhang, L.; Han, X.; Li, C.; Yan, Y.; Xing, L.; Si, M.; Yang, B.; Cheng, L.; et al. LPS-Induced Mitochondrial Damage via SLC41A1-Mediated Magnesium Ion Efflux Leads to the Pyroptosis of Dental Stem Cells. *Adv. Sci.* **2025**, *12*, e05666. [CrossRef] [PubMed]
16. Zuo, J.; Guo, Q.; Fan, Y.; Fu, X.; Zhang, F.; Zhu, X.; Ning, C.; Kong, Y.; Yu, P.; Zheng, J. Self-powered intracellular nanogenerator attenuates inflammatory osteolysis through mitochondrial MRS2/Mg(2+)-mediated macrophage repolarization and osteoclastogenesis inhibition. *Mater. Today Bio* **2025**, *33*, 102050. [CrossRef] [PubMed]
17. Gerwin, N.; Bendele, A.M.; Glasson, S.; Carlson, C.S. The OARSI histopathology initiative—Recommendations for histological assessments of osteoarthritis in the rat. *Osteoarthr. Cartil.* **2010**, *18*, S24–S34. [CrossRef] [PubMed]
18. Liu, Y.; Liu, Y.; Zhang, N.; An, H.; Mi, L.; Gao, Y.; Xu, K. Mitochondrial transplantation for osteoarthritis: From molecular mechanisms to clinical translation. *Front. Immunol.* **2026**, *17*, 1716906. [CrossRef] [PubMed]
19. Liu, G.; Li, D.; Wei, Z.; Xia, R.; Liu, Y.; Zhang, Q.; An, S.; Wang, D. HIF-1α-centered metabolic reprogramming in osteoarthritis: Cell type-specific effects and intercellular crosstalk among chondrocytes, BMSCs, and macrophages. *Front. Immunol.* **2026**, *17*, 1915008. [CrossRef] [PubMed]
20. Wu, Z.; Wang, Y.; Zhu, M.; Lu, M.; Liu, W.; Shi, J. Synovial microenvironment in temporomandibular joint osteoarthritis: Crosstalk with chondrocytes and potential therapeutic targets. *Life Sci.* **2024**, *354*, 122947. [CrossRef] [PubMed]
21. Zhou, R.; Fu, W.; Vasylyev, D.; Waxman, S.G.; Liu, C.J. Ion channels in osteoarthritis: Emerging roles and potential targets. *Nat. Rev. Rheumatol.* **2024**, *20*, 545–564. [CrossRef] [PubMed]
22. Yao, H.; Xu, J.K.; Zheng, N.Y.; Wang, J.L.; Mok, S.W.; Lee, Y.W.; Shi, L.; Wang, J.Y.; Yue, J.; Yung, S.H.; et al. Intra-articular injection of magnesium chloride attenuates osteoarthritis progression in rats. *Osteoarthr. Cartil.* **2019**, *27*, 1811–1821. [CrossRef] [PubMed]
23. Macchi, V.; Stocco, E.; Stecco, C.; Belluzzi, E.; Favero, M.; Porzionato, A.; De Caro, R. The infrapatellar fat pad and the synovial membrane: An anatomo-functional unit. *J. Anat.* **2018**, *233*, 146–154. [CrossRef] [PubMed]
24. Cao, Y.; Rao, C.; Du, Z. The SLC41 Family of Magnesium Transporters: Molecular Regulators of Magnesium Homeostasis and Their Multifaceted Roles in Human Diseases. *Int. J. Mol. Sci.* **2026**, *27*, 1673. [CrossRef] [PubMed]
25. Wang, L.; Yan, Z.; Yalavarthi, S.; Abdul-Rashid, Y.; Parker, K.; Nowlin, K.; Li, E.; Mack, J.; Wei, J.; Vu, H.; et al. Macrophage-Targeted Magnesium Ion-Nourisher for NLRP3 Inflammasome Inhibition to Enhance Liver Inflammatory Disease Treatment. *Adv. Sci.* **2026**, *13*, e13798. [CrossRef] [PubMed]
26. Tseng, A.P.; Wei, H.; Hsiung, N.; Chen, S.H.; Chen, H.Y.; Cheng, F.C. SLC41A1, a Na^+/Mg^{2+} exchanger, is downregulated during exercise. *BioMed. Rep.* **2014**, *2*, 599–601. [CrossRef] [PubMed]

27. Yu, N.; Jiang, J.; Yu, Y.; Li, H.; Huang, X.; Ma, Y.; Zhang, L.; Zou, J.; Zhang, B.; Chen, S.; et al. SLC41A1 knockdown inhibits angiotensin II-induced cardiac fibrosis by preventing Mg(2+) efflux and Ca(2+) signaling in cardiac fibroblasts. *Arch. Biochem. Biophys.* **2014**, *564*, 74–82. [CrossRef] [PubMed]
28. Tsao, Y.T.; Shih, Y.Y.; Liu, Y.A.; Liu, Y.S.; Lee, O.K. Knockdown of SLC41A1 magnesium transporter promotes mineralization and attenuates magnesium inhibition during osteogenesis of mesenchymal stromal cells. *Stem Cell Res. Ther.* **2017**, *8*, 39. [CrossRef] [PubMed]
29. Zhu, X.; Lee, C.W.; Xu, H.; Wang, Y.F.; Yung, P.; Jiang, Y.; Lee, O.K. Phenotypic alteration of macrophages during osteoarthritis: A systematic review. *Arthritis Res. Ther.* **2021**, *23*, 110. [CrossRef] [PubMed]
30. Usher, K.M.; Zhu, S.; Mavropalias, G.; Carrino, J.A.; Zhao, J.; Xu, J. Pathological mechanisms and therapeutic outlooks for arthrofibrosis. *Bone Res.* **2019**, *7*, 9. [CrossRef] [PubMed]
31. Chen, G.; Du, Z.; Rao, C. SLC41A1 overexpression correlates with immune cell infiltration in HCC and promotes its malignant progression. *Int. J. Med. Sci.* **2024**, *21*, 3069–3082. [CrossRef] [PubMed]
32. Yan, B.; Li, Y.; Liu, Y.; Zhang, Y.; Liu, S.; Wang, F.; Gao, L. Targeted soluble epoxide hydrolase inhibits M1 macrophage polarization to improve cartilage injury in temporomandibular joint osteoarthritis. *J. Transl. Med.* **2025**, *23*, 969. [CrossRef] [PubMed]
33. Zhang, Z.; Xie, S.; Qian, J.; Gao, F.; Jin, W.; Wang, L.; Yan, L.; Chen, H.; Yao, W.; Li, M.; et al. Targeting macrophagic PIM-1 alleviates osteoarthritis by inhibiting NLRP3 inflammasome activation via suppressing mitochondrial ROS/Cl(-) efflux signaling pathway. *J. Transl. Med.* **2023**, *21*, 452. [CrossRef] [PubMed]
34. Fan, Y.; Niu, Z.; Yin, L.; Yao, L.; Ding, S.; Tong, Y.; Wang, J.; Hong, Z.; Chen, J.; Zhang, Q.; et al. Membrane biomimetic nanoenzyme-incorporated hybrid glycyrrhizic acid hydrogel for precise mitochondrial ROS scavenging for osteoarthritis treatment. *Mater. Today Bio* **2025**, *32*, 101778. [CrossRef] [PubMed]
35. Li, Z.; Lu, H.; Fan, L.; Ma, X.; Duan, Z.; Zhang, Y.; Fu, Y.; Wang, S.; Guan, Y.; Yang, D.; et al. Microneedle-Delivered PDA@Exo for Multifaceted Osteoarthritis Treatment via PI3K-Akt-mTOR Pathway. *Adv. Sci.* **2024**, *11*, e2406942. [CrossRef] [PubMed]
36. Liu, H.; Li, T.; Zhao, S.; Qiao, X.; Zhang, Q.; He, Y.; Xie, Y.; Hu, B.; Bi, H.; Miao, W.; et al. A Comprehensive Review of Metal-Based Nanozymes for ROS Scavenging and Therapeutic Applications in Osteoarthritis. *ACS Biomater. Sci. Eng.* **2026**, *12*, 1991–2016. [CrossRef] [PubMed]
37. Li, J.; Ke, H.; Wu, D.; Shao, Y.; Wen, Z.; Zhong, S.; Lei, X.; Li, J.; Xie, D.; Zeng, C. Bilayer book- like decellularized extracellular matrix scaffold with bioactive coatings for rotator cuff repair. *Mater. Today Bio* **2025**, *33*, 102038. [CrossRef] [PubMed]
38. Zhao, J.; Wu, H.; Wang, L.; Jiang, D.; Wang, W.; Yuan, G.; Pei, J.; Jia, W. The beneficial potential of magnesium-based scaffolds to promote chondrogenesis through controlled Mg(2+) release in eliminating the destructive effect of activated macrophages on chondrocytes. *Biomater. Adv.* **2022**, *134*, 112719. [CrossRef] [PubMed]

Disclaimer/Publisher's Note: The statements, opinions and data contained in all publications are solely those of the individual author(s) and contributor(s) and not of MDPI and/or the editor(s). MDPI and/or the editor(s) disclaim responsibility for any injury to people or property resulting from any ideas, methods, instructions or products referred to in the content.